Solvent effect on the absorption spectra of coumarin 120 in water: A combined quantum mechanical and molecular mechanical study

Tetsuya Sakata,[1] Yukio Kawashima,[1,2,a)] and Haruyuki Nakano[1]
[1]*Department of Chemistry, Graduate School of Sciences, Kyushu University, Fukuoka 812−8581, Japan*
[2]*Institute of Advanced Research, Kyushu University, Fukuoka 812−8581, Japan*

(Received 18 June 2010; accepted 7 October 2010; published online 3 January 2011)

The solvent effect on the absorption spectra of coumarin 120 (C120) in water was studied utilizing the combined quantum mechanical/molecular mechanical (QM/MM) method. In molecular dynamics (MD) simulation, a new sampling scheme was introduced to provide enough samples for both solute and solvent molecules to obtain the average physical properties of the molecules in solution. We sampled the structure of the solute and solvent molecules separately. First, we executed a QM/MM MD simulation, where we sampled the solute molecule in solution. Next, we chose random solute structures from this simulation and performed classical MD simulation for each chosen solute structure with its geometry fixed. This new scheme allowed us to sample the solute molecule quantum mechanically and sample many solvent structures classically. Excitation energy calculations using the selected samples were carried out by the generalized multiconfigurational perturbation theory. We succeeded in constructing the absorption spectra and realizing the red shift of the absorption spectra found in polar solvents. To understand the motion of C120 in water, we carried out principal component analysis and found that the motion of the methyl group made the largest contribution and the motion of the amino group the second largest. The solvent effect on the absorption spectrum was studied by decomposing it in two components: the effect from the distortion of the solute molecule and the field effect from the solvent molecules. The solvent effect from the solvent molecules shows large contribution to the solvent shift of the peak of the absorption spectrum, while the solvent effect from the solute molecule shows no contribution. The solvent effect from the solute molecule mainly contributes to the broadening of the absorption spectrum. In the solvent effect, the variation in C–C bond length has the largest contribution on the absorption spectrum from the solute molecule. For the solvent effect on the absorption spectrum from the solvent molecules, the solvent structure around the amino group of C120 plays the key role. © *2011 American Institute of Physics*. [doi:10.1063/1.3506616]

I. INTRODUCTION

Coumarin 120 (C120, 7-amino-4-methyl-1,2-benzopyrone, Fig. 1) is the basic molecule in the 7-aminocoumarin family. The compounds 7-aminocoumarins, or 4-methyl-7-diethylaminocoumarins, are the most featured dyes among the coumarin family. The substitution at the 7-position with an electron-donating group enhances the fluorescence of the dye, which leads to their wide application in blue–green laser dyes and fluorescence probes. Furthermore, 7-aminocoumarin dyes are applied to study solvatochromic properties since the large Stokes shifts of these molecules are very sensitive to the polarity and viscosity of the surrounding solvent environment. Hence, the photophysics of these dyes has been studied intensively.[1–24] In spite of the numerous studies and wide applications of 7-aminocoumarins, further investigation of the excited states is essential. The nonradiative deactivation mechanism of 7-aminocoumarins has been debated for the past two decades. The first model describes the nonradiative deactivation process as the 7-aminocoumarin forms the so-called twisted intramolecular charge transfer state from the S_1 singlet excited state.[1] The second is the so-called open–closed umbrellalike motion mechanism.[2] This mechanism ascribes the internal conversion process to a structural change of the amino group from a planar N^+-aromatic configuration (with sp^2 hybridization for the nitrogen atom) to a pyramidal N-aromatic configuration (with sp^3 hybridization for the nitrogen atom). For C120,[8] it is known that the nonradiative deactivation process differs in polar and nonpolar solvents. Thus, it is essential to elucidate the solvent effect of the excited states.

Since the pioneering work of Warshel and Levitt,[25] combined quantum mechanical/molecular mechanics (QM/MM) methods have been successful in tackling the electronic structure calculation of large-scale systems. Especially in the last decade, QM/MM methods have been applied to various problems such as chemical reactions in enzyme or solvent environments.[26,27] In QM/MM methods, the calculated molecular system is divided into at least two different subsystems: one subsystem where the quantum effect that must be included is treated by QM and the other subsystem includes the environmental effect that is treated by molecular

a)Author to whom correspondence should be addressed. Electronic mail: snow@ccl.scc.kyushu-u.ac.jp.

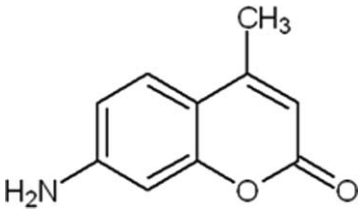

FIG. 1. Structure of C120.

mechanics (MM). Efforts were made to obtain the average properties of the electronic excited states by using the QM/MM method and treating solvents by MM.[26–29] Molecular dynamics (MD) simulation combined with the QM/MM method is a powerful tool for studying the electronic structure of molecules in solution. The solute and solvent molecules are sampled simultaneously; the former is sampled by quantum mechanical calculation and the latter by classical simulation. Both the Car–Parrinello and Born–Oppenheimer MD simulations employing the QM/MM method were applied to study the excited state structure in solvents; however, it is still difficult to sample enough solvent structures to obtain converged average properties. In these methods, the excitation energy corresponding to the peak of the spectrum is obtained, but the entire spectrum cannot be constructed. The solvent effect leads to a red or blue shift and to broadening of the spectrum. Thus, to fully understand the effect of the environment, construction of the entire absorption spectrum is necessary.

In a previous work,[30] we executed a classical Monte Carlo simulation and obtained enough snapshots to obtain average solvent properties. We next chose 400 configurations and performed quantum mechanical calculations for these configurations, which we used to calculate the average physical properties. We applied this scheme to the first excited state of formaldehyde and calculated the absorption spectra in water. We succeeded in constructing the absorption spectra and obtaining the converged absorption spectra peak and blue shift in water. The use of full classical simulation for sampling the solvent structure enabled us to obtain the average property over many solvent structures. Many studies follow a similar scheme.[31–35] Sanchez *et al.* used classical MD simulation to calculate the averaged value of the solvent electrostatic potential and perform quantum mechanical calculations using this averaged mean field.[36] This reduces the number of quantum mechanical calculations; however, it cannot construct the entire spectrum. Warshel and co-workers developed the adiabatic charge approach, which uses a mapping potential, to execute free energy perturbation calculations.[37,38] Pulay *et al.* recently developed a similar method, which uses expansion of electric potential generated by classical simulation.[39] In previous sampling schemes, although the solvent structures are well sampled, the solute molecules are not sampled. In classical simulation, the solute molecules are fixed, and this is not realistic, in particular for large solute molecules. Moreover, the geometry affects the absorption spectrum and thus quantum mechanical treatment is necessary to sample the solute structures. Levy and co-workers have employed a flexible model for the solute molecule to sample the solute structure, but the solute molecule was sampled classically.[31,32] Obtaining the free energy utilizing QM/MM free energy perturbation simulation faced the similar problem. Simulation fixing the solute molecule fails to include the entropic contribution of the solute molecule, which cannot be estimated by harmonic approximation.[40] Many methods are developed to overcome this problem.[41–51]

To overcome the drawback of the previous method, we introduced a new efficient sampling scheme to obtain average physical properties. We combined this new scheme with a multireference perturbation theory that we developed. The multireference perturbation theory based on multiconfigurational reference functions has become a practical tool for studying the electronic structures of low-lying excited states. The multireference Møller–Plesset perturbation theory[52–54] and the multiconfigurational quasidegenerate perturbation theory[55,56] succeeded in describing the excited states of π-conjugated systems and taking into account both static and dynamic electron correlation.[57–64] These methods include valence π and π^* orbitals in the active space of the reference complete active space self-consistent field (CASSCF) wave function to perform calculations of the $\pi \rightarrow \pi^*$ excited states. However, the use of the CASSCF wave function limits the application of these methods to large π-conjugated systems since the active space dimension grows enormously with the number of active orbitals and electrons. To avoid this drawback, a perturbation theory using general multiconfiguration SCF wave functions as reference functions [general multiconfigurational quasidegenerate perturbation theory and general multiconfigurational-perturbation theory (GMC-PT)] was developed.[65,66] This method enables us to do calculations using larger active space, which leads to a broader application. We have succeeded in obtaining accurate excitation and fluorescence energies of coumarin 120 and 151 in a previous work of ours.[24]

The electrons of the solvent molecules may play an important role in the excitation process, where they instantly respond to the change of the solute electronic structure.[25,67,68] In the previous work,[30] we investigated the effect of the solvent MM induced dipoles, which were introduced in the first QM/MM calculations,[25] on the absorption spectra. However, the effect of the induced dipoles was not large in our previous work; thus, we do not introduce them in this work.

In this article, we aim to elucidate the character of the first singlet excited state of C120 in water solution. Introducing a new sampling scheme, we aim to construct the absorption spectra in water and understand the correlation between the absorption spectra and solute and solvent structures. This article is organized as follows. The sampling scheme and computational details are described in Sec. II. The results of the calculations are discussed in Sec. III.

II. METHODS AND COMPUTATIONAL DETAILS

To overcome the drawback of the previous method, where we sampled the solvent molecules using classical simulation, we introduce a new efficient sampling scheme to obtain average physical properties. The new sampling scheme is described in Fig. 2. In our new sampling scheme, we sample

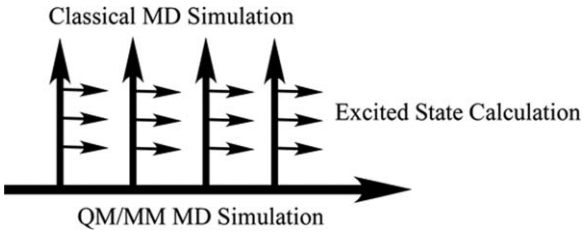

FIG. 2. The new sampling scheme.

the structure of the solute and solvent molecules separately. The scheme is as follows:

1. Execute a QM/MM MD simulation, where we sample the solute molecule in solution.
2. Sample random solute structures randomly from simulation 1 and then perform a classical MD simulation for each chosen solute structure with its geometry fixed.
3. Sample solvent structures from simulation 2 and perform a quantum chemical calculation of the excitation energies with the randomly chosen solvent structures sampled from this classical simulation.
4. Construct the absorption spectra from the ensemble of the calculated excitation energies in 3.

This sampling scheme is a combination of QM/MM MD simulation and the previous sampling scheme where we sampled only the solvent molecules using classical simulation. This new scheme allows us to sample the solute molecule quantum mechanically and sample many solvent structures.

First, to check the accuracy of our calculation, we computed the excitation energy of the first singlet excited state of C120 in the gas phase using the GMC-PT[65,66] method. 20 electrons and 17 orbitals were necessary to include all valence π, π^*, and n orbitals for our GMC-PT calculation. Geometry was optimized at the B3LYP (Refs. 69–71) level, and cc-pVDZ (Ref. 72) is used as the basis set for all calculations.

We applied QM/MM calculations to C120 in water, where the solute, C120, was treated quantum mechanically and the solvent water molecules were treated molecular mechanically. First, we executed the QM/MM MD simulation of the ground state of C120 in 417 water molecules with a spherical boundary for 40 000 steps with a 0.5 fs time step. C120 was treated at the B3LYP level. Next, we randomly chose 65 solute structures from the QM/MM MD simulation and solvated them in a 30 Å × 30 Å × 30 Å water cube. We performed classical MD simulation for each chosen C120–water system fixing the geometry of the solute molecule for one million steps with a 0.5 fs time step. The periodic boundary condition was applied to classical MD simulation using the particle-mesh Ewald method[73] for treating the long-range Coulomb force with 808 water molecules. The leapfrog Verlet algorithm was used for integration of the equation of motion. Finally, we chose four C120–water snapshot structures from each 65 classical MD simulations and computed the excitation energies of each snapshot structure. Thus, the total number of excited state calculations was 260. GMC-PT was used for excited state calculations of the solute C120 molecule, whereas water molecules were treated molecular mechanically. Dunning's cc-pVDZ was used for all QM calculations, and CHARMM27 force field parameters (Ref. 74) and TIP3P water parameters[75] were used for MM calculations. CHARMM (Ref. 76) and Q-CHEM (Ref. 77) programs were employed for the QM/MM MD simulation, NAMD (Ref. 78) program was employed for classical MD simulation for sampling the solvents, and the GAMESS (Ref. 79) package was used to carry out GMC-PT calculations.

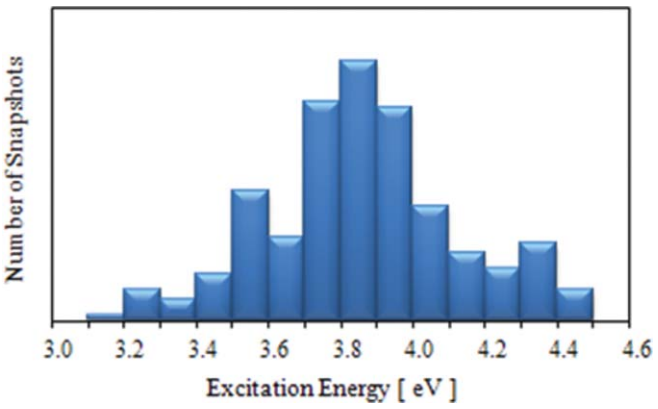

FIG. 3. The constructed absorption spectrum.

III. RESULTS AND DISCUSSION

A. The absorption spectra and average properties

We constructed the absorption spectrum originating from the first excited state of C120 by applying QM/MM calculations to obtained snapshots from the simulation. The spectrum is a histogram of the calculated excitation energies of chosen snapshots. The constructed absorption spectrum illustrated in Fig. 3 ranges from 3.15 to 4.48 eV. The peak of this histogram is found between 3.80 and 3.90 eV and agrees well with the average excitation energy of 3.86 eV. The spectrum is well described as a Gaussian distribution with the peak at the average excitation energy. The calculated excitation energy in gas phase is 3.89 eV. This excited state has a $\pi \rightarrow \pi^*$ character. Our calculation obtained a red shift in water solution. Hereafter, we focus on this red shift of the absorption spectrum in water to discuss the solvent effect.

In our sampling scheme, we sampled the solute and solvent structures separately. This enabled us to decompose the effect of the solvent on the absorption spectra into two components. First is the solvent effect, which is caused by the geometrical distortion of the solute from the gas phase structure. Second is the electric field effect of the solvent molecules. Here, we decomposed the shift of the absorption spectrum into two components. We denote the shift from the distortion of the solute molecule as ΔE_1 and the shift from the field effect of the solvent molecules as ΔE_2. This decomposition allowed us to seek the origin of the shape of the spectrum, which cannot be done in the previous QM/MM sampling scheme. ΔE_1 and ΔE_2 are obtained as

$$\Delta E_1 = \text{Gas(Equilibrium Geometry)} - \text{Gas(QM/MMMD)}$$

and

$$\Delta E_2 = \text{Gas(QM/MM MD)} - \text{Water(QM/MM MD + classical MD)},$$

respectively, where Gas(Equilibrium Geometry), Gas(QM/MM MD), and Water(QM/MM MD + classical MD) correspond to excitation energy calculated at gas phase optimized structure, gas phase excitation energy calculated at the solute structure obtained from the QM/MM MD simulation (solvent molecules excluded), and QM/MM excitation energy calculated at the solute structure obtained from the QM/MM MD simulation and solvent structure obtained from the classical simulation, respectively. The total solvent shift of the absorption spectra is

$$\Delta E = \Delta E_1 + \Delta E_2.$$

The calculated shift in the absorption spectra is summarized in Table I. The average of the total solvent shift ΔE is 0.03 eV and its standard deviation 0.27 eV. The average of ΔE_1, the solvent shift from the solute molecule, and ΔE_2, the solvent shift originating from the solvent molecules, is 0.00 and 0.03 eV, respectively. The solvent effect from the solute molecules shows no contribution to the shift, while the contribution from the solvent molecules shows large contribution to the solvent shift. Thus, we found that the red shift originates from the field effect of the solvent molecules and the effect of the solute molecules does not affect the peak of the spectrum. The standard deviations for the two shifts are 0.26 and 0.12 eV, respectively. This shows that the thermal fluctuation of ΔE_1 is larger than ΔE_2. The standard deviation of ΔE_1 is similar to the standard deviation of the total shift ΔE. The contribution of ΔE_1 and ΔE_2 to the total shift ΔE may be seen in the plots in Figs. 4(a) and 4(b), respectively. The plot in Fig. 4(a) shows a large correlation between ΔE_1 and ΔE. Thus, the broadening of the spectrum comes from the fluctuation of the solute geometry. In Fig. 4(b), ΔE_2 is mainly found in the upper region of the plot, which shows that the field effect leads to a red shift, whereas the effect of the solute geometry leads to both red and blue shifts.

B. Analysis of the solute C120 motion in water

To study the solute motion in water, we carried out principal component analysis (PCA) of the solute structures sampled from QM/MM MD. PCA transforms a number of possibly correlated variables into a smaller number of uncorrelated variables called principal components. In our study, we transform possibly correlated atomic motions into a smaller number of molecular motions. We took the average among the solute samples from QM/MM simulations. We collected samples for every ten steps from the QM/MM MD. Thus, a total of 4000 samples were used for PCA. Next, we constructed a variance–covariance matrix and diagonalized it. Here, we removed all six degrees of freedom of the center of mass: three for translation and three for rotation. The obtained eigenvectors correspond to the personal component (PC) axes. The first PC represents the largest motion of C120. The ratios of the contribution, namely, the ratios of the eigenvalues of the first five principal components are 45.2%, 34.2%, 5.7%, 3.1%, and 2.1%. Thus, it can be said that the first two PCs make the dominant contribution to the solute motion. Later on, we focus on the molecular motion described by the first principal component (PC1) and second principal component (PC2) axes.

To study the motion of the atom in C120, the correlation coefficients between the motion of each atoms in C120 molecule and the first two PCs were calculated. The calculated coefficients are listed in Table II. Motion of each atom is decomposed in x, y, and z directions. The atom numbering is illustrated in Fig. 5. Every C120 snapshot is rotated to lie mostly on the $x-y$ plane. The hydrogens of methyl group have the large contributions in both of the PCs. The hydrogens of amino group also have large contributions in both of the PCs. To visualize these motion of the atoms, we vectorize the correlation coefficients of each atom in the x, y, and

TABLE I. The average and standard deviation of the total, solute molecule originated, and the solvent molecules originated solvation shift of the absorption spectra.

	Average value	Standard deviation
ΔE	+0.03 (3.86 eV)	0.27
ΔE_1	±0.00	0.26
ΔE_2	+0.03	0.12

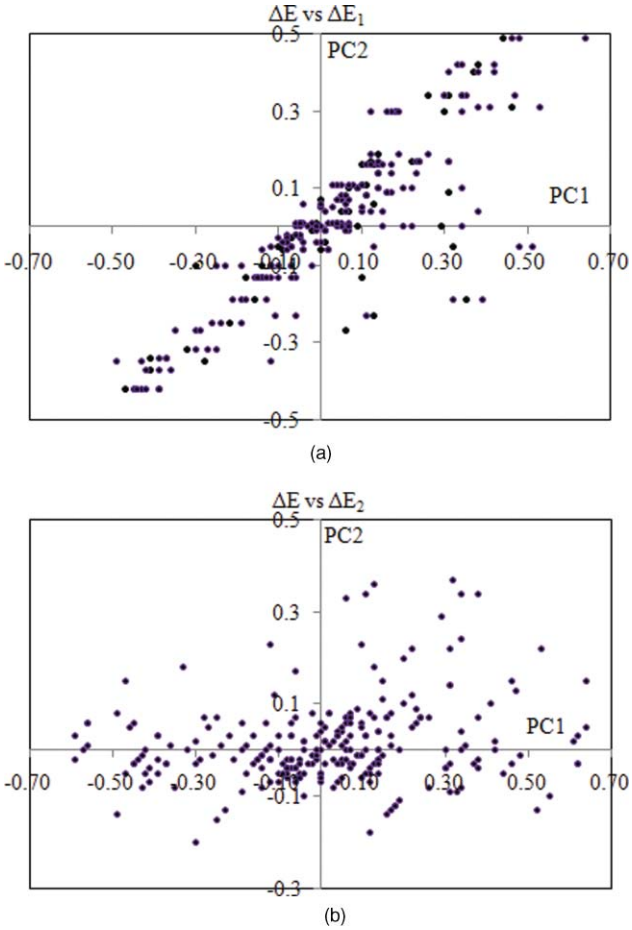

FIG. 4. Plot of the red shift value of 260 snapshots: (a) ΔE vs ΔE_1 and (b) ΔE vs ΔE_2.

TABLE II. Correlation coefficients between the motion of the each atom in C120 molecule, and the first and second principal component (PC). The motion of each atom is decomposed in x, y, and z direction.

	PC1			PC2		
Atom no.	x	y	z	x	y	z
1	0.112	−0.033	−0.085	−0.004	0.011	0.001
2	−0.042	0.027	0.057	−0.019	0.016	0.002
3	−0.083	0.085	0.100	−0.069	0.025	0.047
4	−0.090	0.093	0.113	−0.096	0.039	0.066
5	−0.050	0.080	0.048	−0.084	0.034	0.068
6	0.021	0.023	−0.018	−0.057	0.029	0.045
7	−0.012	0.009	0.023	0.002	−0.009	−0.016
8	−0.042	0.048	0.036	−0.064	0.025	0.048
9	0.033	−0.005	−0.035	−0.032	−0.003	0.031
10	−0.068	0.071	0.067	−0.045	0.005	0.024
11	−0.033	0.050	0.042	−0.024	0.005	0.016
12	0.055	−0.038	−0.064	−0.041	0.043	0.031
13	0.031	0.025	−0.049	−0.036	0.034	0.026
14	0.017	−0.007	−0.042	0.070	−0.071	−0.014
15	0.016	−0.067	−0.068	0.121	0.007	−0.084
16	0.207	−0.102	−0.199	−0.036	0.008	−0.011
17	0.292	−0.256	−0.263	−0.124	0.051	0.085
18	0.022	−0.060	0.029	0.165	−0.057	−0.126
19	0.072	−0.044	−0.077	0.001	0.015	−0.021
20	0.952	−0.412	−0.789	−0.211	−0.899	0.516
21	−0.247	0.980	−0.155	0.941	0.124	−0.932
22	−0.763	−0.676	0.897	−0.601	0.721	0.289

z direction, on an assumption that the correlation coefficient vector, namely, the coefficients in x, y, and z direction, itself describes the direction of the motion for atoms along PC1 and PC2. The motion vectors constructed from the correlation coefficients are illustrated in Fig. 6. Figures 6(a) and 6(b) show the motion along the PC1 and PC2 directions, respectively. For PC1, the motion is described as an open−close motion of a book, where C5−C4−C3−O10 works as the spine. For PC2, we could not classify the entire motion.

To decompose the entire motion of C120 in water, we calculated the correlation coefficients between some typical motions of C120 and the first two PCs. The calculated correlation coefficients are shown in Table III. We selected the open–close conversion of the amino group, the rotation of the amino group around the C1−N15 bond, the bending motion of the C13=O14 bond against the coumarin

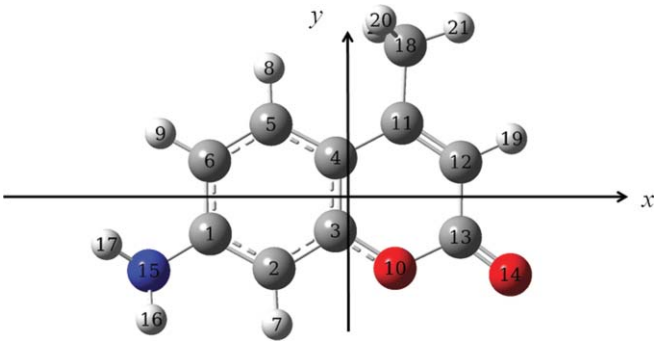

FIG. 5. The atom numbering of C120.

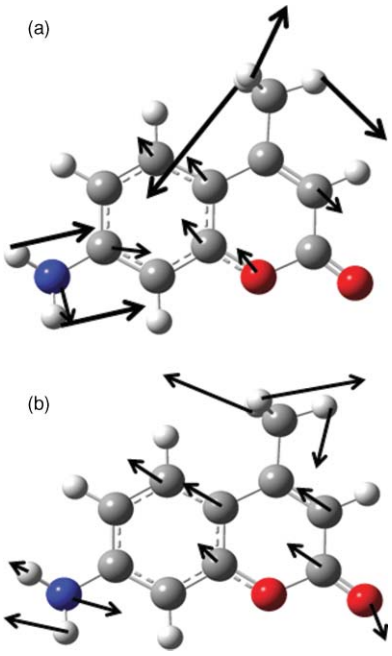

FIG. 6. The vectorized data of the correlation coefficients of between atoms and (a) PC1 and (b) PC2.

ring, the out-of-plane bending of C3−O10−C13, the rotation of the methyl group around the C11−C18 bond, and the end-to-end distance between the hydrogen atoms of the amino group and the hydrogen atoms of the methyl group, which is the coupling between motions of the methyl group and the amino group, to compare with the two PCs. For PC1, the correlation coefficients between the open–close conversion of the amino group, the rotation of the amino group around the C1−N15 bond, the bending motion of the C13=O14 bond against the pyrone ring, the out-of-plane bending of C3−O10−C13, rotation of the methyl group around C11−C18 bond, and the end-to-end distance between the hydrogen atoms of the amino group and the hydrogen atoms of the methyl group were −0.270, −0.067, −0.029, −0.052, 0.185, and 0.775, respectively. The largest coefficient was found in the end-to-end distance between the hydrogens of the amino and methyl groups. The open−close motion of the amino group and the rotation of the methyl group also have correlation with PC1.

For PC2, the correlation coefficients between the open–close conversion of the amino group, the rotation of the amino group around the C1−N15 bond, the bending motion

TABLE III. Correlation coefficients between typical motions of the C120 molecule and the first and second principal components.

	PC1	PC2
Open−close motion of amino group	–0.270	0.142
Rotation of amino group	–0.067	0.088
Bending motion of C = O	–0.029	0.044
Out-of-plane bending of –O–	–0.052	–0.018
Rotation of methyl group	0.185	0.971
End-to-end distance between CH_3 and NH_2	0.775	–0.563

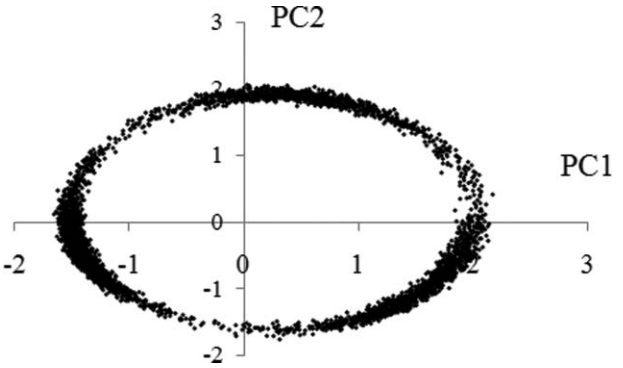

FIG. 7. Plot of 4000 points on the first and second principal component axes plane.

of the C13=O14 bond against the pyrone ring, the out-of-plane bending of C3−O10−C13, rotation of the methyl group around the C11−C18 bond, and the end-to-end distance between the hydrogen atoms of the amino group and the hydrogen atoms of the methyl group were 0.142, 0.088, 0.044, −0.018, 0.971, and −0.563, respectively. The rotation of the methyl group made the dominant contribution. The correlation coefficient was close to 1.0. The open−close motion of the amino group and the end-to-end distance between hydrogen atoms of the amino and methyl groups also contribute to the motion along PC2.

We plotted 4000 points on the PC1 and PC2 planes. The plot is shown in Fig. 7. It can be seen that the plot can be divided into three clusters: around (1.5, −1.5) on the PC1 and PC2 plane, around (0.0, 2.0), and (1.5, −1.0). This can be explained by the rotation of the methyl group. There exists three stable points, every 120° in the rotation of the methyl group, due to the steric effect of the hydrogen atoms. Since the two PCs dominated the entire motion of C120 in water, it could be concluded that the motion of the methyl groups mainly contributed to the entire molecular motion with the motion of the amino group.

C. The origin of the solvent effect on the absorption spectra from the solute

To elucidate the origin of the solvent effect on the absorption spectra from the solute, we calculated the correlation coefficients between the various properties and ΔE_1.

The correlation coefficients between ΔE_1 and the two PCs are listed in Table IV. For ΔE_1, the correlation coefficients between PC1 and PC2 were 0.055 and −0.134, respectively. PC2 had a larger coefficient than PC1, but neither PC contributed much to ΔE_1.

We next calculated the correlation between ΔE_1 and typical motions of C120 to study the PCs mentioned in Sec. III B. The correlation coefficients between ΔE_1 and typical motions of C120 are shown in Table V. For ΔE_1, the correlation coefficients between the open−close conversion of the amino group, the rotation of the amino group around the C1−N15 bond, the bending motion of the C13=O14 bond against the pyrone ring, the out-of-plane bending of C3−O10−C13, rotation of the methyl group around the C11−C18 bond, and the end-to-end distance between the hydrogen atoms of the amino group and the hydrogen atoms of the methyl group were 0.099, 0.012, −0.133, −0.153, 0.109, and −0.032, respectively. There was no typical motion that showed large correlation with ΔE_1. The out-of-plane bending of C3−O10−C13 and the bending motion of the C13=O14 bond against the pyrone ring showed larger correlation compared to other motions.

TABLE IV. Correlation coefficients between the solvation shift of the absorption spectraand the principal component axes.

	ΔE_1	ΔE_2
PC1	0.055	0.204
PC2	–0.134	0.192

TABLE V. Correlation coefficients between the solvation shift of the absorption spectra and typical motions of C120.

	ΔE_1	ΔE_2
Open−close motion of amino group	0.099	− 0.116
Rotation of amino group	0.012	0.214
Bending motion of C=O	− 0.133	0.005
Out-of-plane bending of –O–	− 0.153	− 0.064
Rotation of methyl group	− 0.109	0.167
End-to-end distance between CH_3 and NH_2	− 0.032	0.012

For further investigation, we calculated the correlation between ΔE_1 and the variation in C120 bond lengths. We selected the bond alternation of the benzene ring, the bond alternation of the pyrone ring (in bonds C4−C11−C12−C13), bond length of C13=O14, bond length of C1−N15, and bond length of C11−C18 to calculate the correlation with ΔE_1. We calculated the bond alternation of C−C bonds in benzene and pyrone rings as follows:

$$\text{Bond alternation} = \frac{\left[\sum_i^N (x_i - 1.40)^2\right]}{N},$$

where N is the number of C−C bonds and x is the C−C bond length. 1.40 means 1.40 Å, which is the bond length of C−C bonds between single and double bonds. The correlation coefficients between ΔE_1 and the bond lengths in C120 are shown in Table VI. For ΔE_1, the correlation coefficients between bond alternation in the benzene ring, bond alternation of the C−C bonds in the pyrone ring, bond length of C13=O14, bond length of C1−N15, bond length of C3−O10, bond length of C13−O10, and bond length of C11−C18 were

TABLE VI. Correlation coefficients between the solvation shift of the absorption spectraand bond lengths of C120.

	ΔE_1	ΔE_2
Bond alternation of the benzene ring of C120	0.243	0.016
Bond alternation in C4−C11−C12−C13	− 0.355	− 0.105
Bond length of C13=O14	0.033	0.025
Bond length of C1−N15	0.156	0.031
Bond length of C3−O10	− 0.226	0.099
Bond length of C13−O10	0.268	0.153
Bond length of C11−C18	− 0.006	0.113

TABLE VII. Correlation coefficients between the solvation shift of the absorption spectra and the distance to the first peak of the radial distribution function between C120 and water in classical simulation.

	ΔE_1	ΔE_2
Distance to the first peak of RDF(N15(C120)−H(Water))	–0.113	0.521
Distance to the first peak of RDF(O14(C120)−H(Water))	–0.077	0.157

0.243, −0.355, 0.033, 0.156, −0.226, 0.268, and −0.006, respectively. The bond alternation of the C−C bonds in the pyrone ring had the largest coefficients. The bond alternation in the benzene ring, the bond length of C3−O10 and bond length of C13−O10 also had large coefficients. The positive sign of the correlation coefficients for bond alternation of the C−C bonds in the benzene ring shows that the bond alternation becomes larger and the negative sign in the pyrone ring shows that the bond alternation becomes smaller. In other words, the aromaticity of the benzene ring became smaller and that of the pyrone ring became larger. This influenced the π orbitals, which play an important role in the $\pi \rightarrow \pi^*$ excitation.

In this study, we found that the variation in bond alternation of benzene and pyrone rings had the largest contribution in the solvent effect on the absorption spectra from the solute molecule.

D. The origin of the solvent effect on the absorption spectra from the solvent molecules

To elucidate the origin of the solvent effect on the absorption spectra from the solvent molecules, we calculated the correlation coefficients between various properties and ΔE_2.

The correlation coefficients between ΔE_2 and the two PCs are shown in Table IV. For ΔE_2, the correlation coefficients between PC1 and PC2 were 0.204 and 0.192, respectively. The motion of the methyl group had the largest contribution to the PCs and the amino group the second largest.

Next, we calculated the correlation between ΔE_2 and typical motions of C120. The correlation coefficients between ΔE_2 and typical motions of C120 are listed in Table V. For ΔE_2, the correlation coefficients between the open−close conversion of the amino group, the rotation of the amino group around the C1−N15 bond, the bending motion of the C13=O14 bond against the pyrone ring, the out-of-plane bending of C3−O10−C13, the rotation of the methyl group around the C11−C18 bond, and the end-to-end distance between the hydrogen atoms of the amino group and the hydrogen atoms of the methyl group were −0.116, 0.214, 0.005, −0.064, 0.167, and 0.012, respectively. The rotation of the amino group had the largest coefficients.

We calculated the correlation between ΔE_2 and C120 bond lengths. The correlation coefficients between ΔE_2 and the bond lengths in C120 are given in Table VI. For ΔE_2, the correlation coefficients between bond alternation in the benzene ring, bond alternation of the C−C bonds in the pyrone ring, bond length of C13=O14, bond length of C1−N15, bond length of C3−O10, bond length of C13−O10, and bond length of C11−C18 were 0.016, −0.105, 0.025, 0.031, 0.099, 0.153, and 0.113, respectively. Compared to ΔE_1, there was no bond length with large coefficients. The bond alternation of the C−C bonds in the pyrone ring has the largest coefficient.

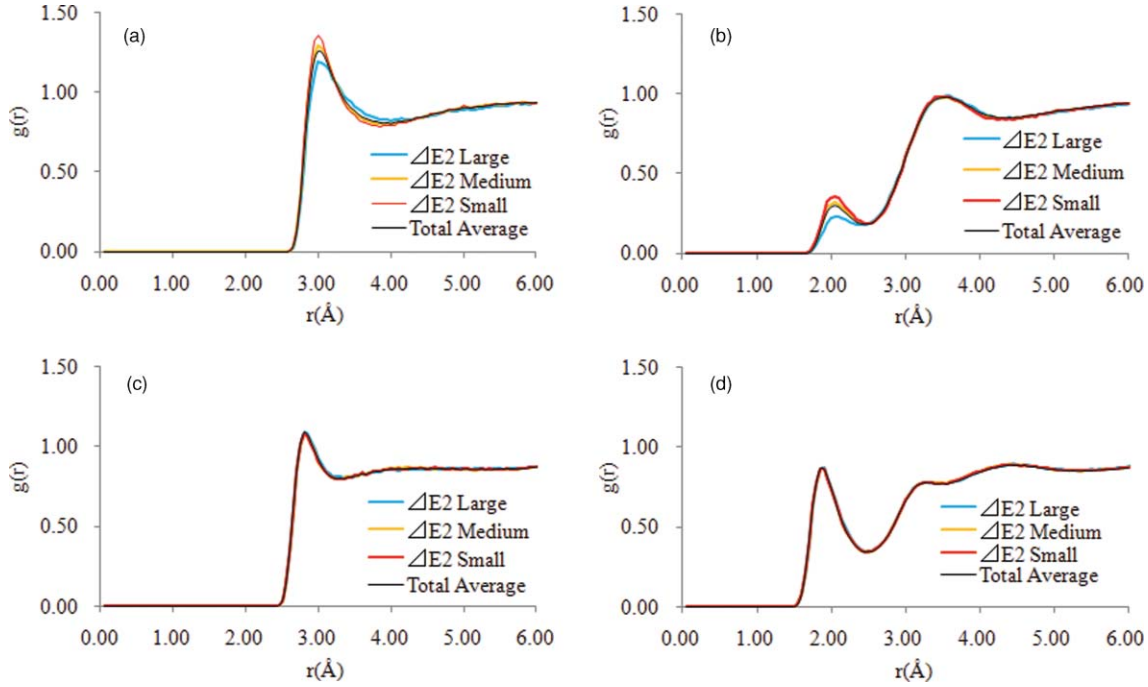

FIG. 8. Radial distribution function (RDF) between (a) the nitrogen atom of the amino group of C120 and the oxygen atom of water molecules, (b) the nitrogen atom of the amino group of C120 and hydrogen atoms of water molecules, (c) the oxygen atom of the carbonyl group of C120 and the oxygen atom of water molecules, and (d) the oxygen atom of the carbonyl group of C120 and hydrogen atoms of water molecules. Blue, yellow, and red lines represent the RDF of snapshots from $\Delta E_2{}^{\text{large}}$, $\Delta E_2{}^{\text{medium}}$, and $\Delta E_2{}^{\text{small}}$. The black line represents the RDF of all snapshots.

To investigate the effect from solvent molecules, we constructed radial distribution functions (RDFs) between C120 and water molecules for 65 classical simulations, where we sampled the solvent structures. We constructed four RDFs for each simulation: between N15 of C120 and the oxygen atom of water [later denoted as RDF(N15(C120)−O(Water))], between N15 of C120 and the hydrogen atoms of water [later denoted as RDF(N15(C120)−H(Water))], between O14 of C120 and the oxygen atom of water [later denoted as RDFO14(C120)−O(Water))], and between O14 of C120 and the hydrogen atoms of water [later denoted as RDF(O14(C120)−H(Water))]. We calculated the correlation between ΔE_2 and the distance to the first peak in RDF(N15(C120)−H(Water)) and RDF(O14(C120)−H(Water)), which are listed in Table VII. For ΔE_2, the correlation coefficients between RDF(N15(C120)−H(Water)) and RDF(O14(C120)−H(Water)) were 0.521 and 0.157, respectively. We found that the distance to the first peak in RDF(N15(C120)−H(Water)) had a large coefficient.

To investigate the relation between ΔE_2 and the solvent structures further, we categorized the RDFs constructed from 65 classical MD simulations according to the value of ΔE_2. Since four snapshots were selected from each classical simulation to calculate the excitation energy, we obtained four ΔE_2 values from each simulation. Here, we assumed that the average of these four ΔE_2 values corresponds to the average of the entire simulation. We categorized snapshots with ΔE_2 smaller than –0.05 eV as $\Delta E_2{}^{\text{small}}$, snapshots with ΔE_2 larger than 0.05 eV as $\Delta E_2{}^{\text{large}}$, and snapshots with ΔE_2 between –0.05 and 0.05 eV as $\Delta E_2{}^{\text{medium}}$. The RDFs constructed with categorized snapshots are depicted in Fig. 8. Figures 8(a)−8(d) illustrate RDF(N15(C120)−O(Water)), RDF(N15(C120)−H(Water)), RDF(O14(C120)−O(Water)), and RDF(O14(C120)−H(Water)), respectively. In the RDFs of O14, the difference between $\Delta E_2{}^{\text{large}}$, $\Delta E_2{}^{\text{medium}}$, $\Delta E_2{}^{\text{small}}$ cannot be seen. On the other hand, differences among the ΔE_2 values can be seen in RDF(N15(C120)−O(Water)) and RDF(N15(C120)−H(Water)). A difference can be seen in the first peak of the RDFs. The first peak of these RDFs becomes larger as ΔE_2 becomes larger. This agrees with the positive correlation coefficients between ΔE_2 and the distance to the first peak of RDF(N15(C120)−H(Water)).

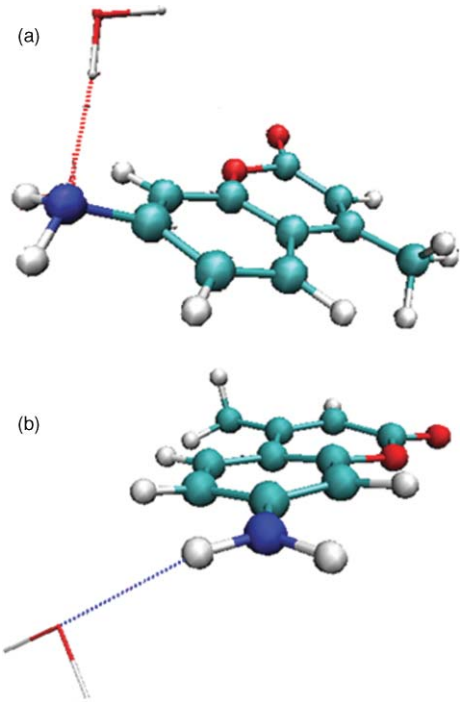

FIG. 9. Typical snapshot structure of C120: (a) pyramidal amino group structure and (b) planar amino group structure.

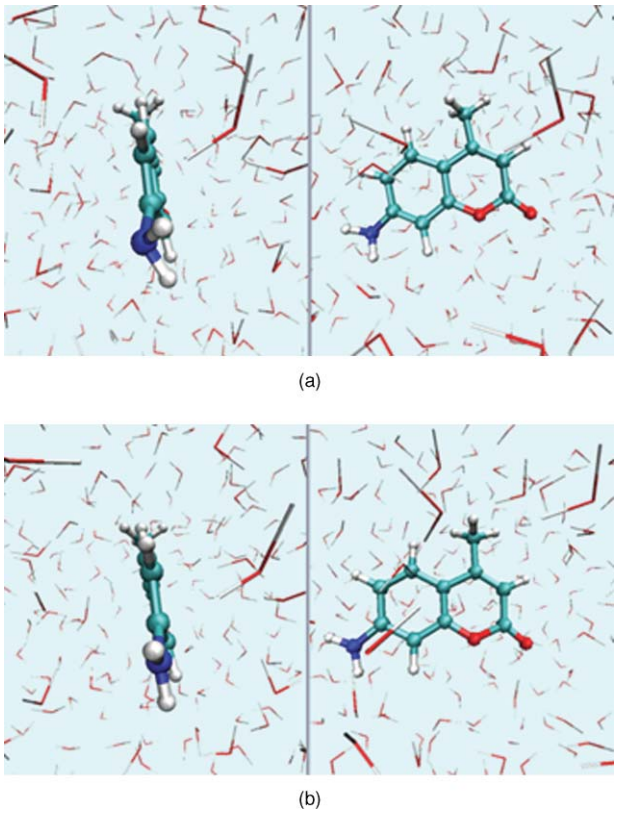

FIG. 10. Snapshot structures chosen from QM/MM MD simulation: (a) C120 with pyramidal amino group structure and (b) C120 with planar amino group structure.

To discuss the differences between solvent structures in detail, we focused on the snapshot structures. The snapshots with a large ΔE_2 red shift have the tendency to form a pyramidal coumarin amino group [Fig. 9(a)] and the solute forms hydrogen bonds with solvents at the nitrogen atom of the amino group. On the other hand, snapshots with a small ΔE_1 red shift have the tendency to form a planar amino group [Fig. 9(b)] and no hydrogen bonds are formed at the nitrogen atom. We selected two snapshot structures: the pyramidal amino group structure at step number 1080 and the planar structure at step number 1260 from QM/MM MD simulation. The snapshot structures are depicted in Fig. 10. The calculated excitation energies and red shift of these two snapshots are listed in Table VIII. The excitation energies calculated with pyramidal structure show small ΔE_2 value, while the planar structure shows a large ΔE_2 value. To understand the difference in the ΔE_2 red shift between the two structures, we focus on the solute–solvent interactions. RDF(N15(C120)−O(Water)) and

TABLE VIII. The solvent shift values of two snapshot structures.

	Pyramidal	Planar
ΔE_2 [eV]	0.00	0.11
Dipole moment (gas/ground state)	5.42	5.35
Dipole moment (gas/excited state)	5.47	5.46
Dipole moment (water/ground state)	6.45	7.06
Dipole moment (water/excited state)	6.50	7.92

RDF(N15(C120)−H(Water)) of the two snapshots are illustrated in Figs. 11(a) and 11(b), respectively. The hydrogen bond from the amino nitrogen to the water hydrogen leads to the peak found as shown in Fig. 11(b) for the pyramidal structure. The first peak for the planar structure is the hydrogen bond from the hydrogen of the amino group to the oxygen of water as described in Fig. 11(a). The solvation structures contribute to the electrostatic effect of the electronic structure of the solute. Thus, the radial distribution function indicates that a hydrogen bond between nitrogen of the amino group and hydrogen of water leads to a large decrease in the ΔE_2 and the hydrogen bond found in the planar structure leads to a large ΔE_2 value. In Table VIII, the dipole moments of the two structures are compared. In the gas phase, where no water molecules are present, the two structures have similar dipole moments in both the ground and first excited states. On the other hand, when the water molecules are present, the dipole moments of both the structures are enlarged. The dipole moment of the planar structure has a larger solvent shift compared to the pyramidal structure. Comparing the dipole moments of the ground and excited states, the excited state of the planar structure has larger dipole moment compared to the ground state, while difference of the dipole moments between two states are small in the pyramidal structure. The planar structure has large dipole moment in the excited state compared to the ground state, which leads to larger stabilization of the excited state compared to the ground state from the solvent effect via the solvent molecules. This stabilization leads to the red shift of the absorption spectrum.

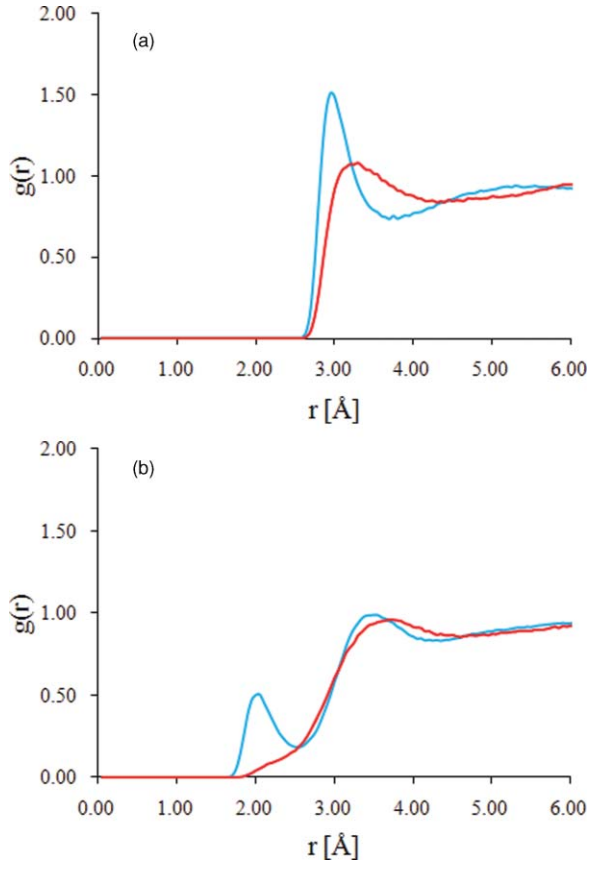

FIG. 11. Radial distribution function between the nitrogen atom of the amino group of C120 and (a) oxygen atom of water molecules and (b) hydrogen atom of water molecules. Blue and red lines correspond to C120 with pyramidal and planar amino groups, respectively.

IV. CONCLUSION

We studied the solvent effect on the absorption spectra of C120 in water. We introduced a new sampling scheme to obtain the average physical properties in solution for QM/MM calculations. We sampled the structure of the solute molecule and solvent molecules separately. First, we carried out a QM/MM MD simulation, where we sampled the solute molecule in solution. Next, we chose arbitrary solute structures from this simulation and performed classical MD simulation for each chosen solute structure with its geometry fixed. This new scheme allows the sampling of the solute molecule quantum mechanically and the sampling of many solvent structures. We succeeded in constructing the absorption spectrum and obtained the red shift of the absorption spectrum found in polar solvents.

To understand the motion of C120 in water, we carried out PCA. We found that the motion of the methyl group makes the largest contribution and the motion of the amino group the second largest.

Taking advantage of our scheme, the solvent effect on the absorption spectrum was decomposed into two components: the effect from the distortion of the solute molecule and the field effect from the solvent molecules. The solvent effect from the solvent molecules shows large contribution to the solvent shift of the peak of the absorption spectrum, while the solvent effect from the solute molecule shows no contribution. The solvent effect from the solute molecule mainly contributes to the broadening of the absorption spectrum. The variation in C–C bond length has the largest contribution in the solvent effect on the absorption spectrum from the solute molecule. For the solvent effect on the absorption spectrum from the solvent molecules, the solvent structure around the amino group of C120 plays the key role.

However, the present study has one drawback. We have not calculated the entire absorption spectrum in the gas phase. The difference among the broadening of the absorption spectra in gas phase and in water is not yet studied. Virshup *et al.* constructed the absorption spectra of green fluorescent protein for both gas phase and in water utilizing QM/MM MD and studied the difference among these two spectra.[80] We next aim to use our new sampling scheme to study the broadening of the absorption spectra as in Ref. 80.

ACKNOWLEDGMENTS

Y.K. was supported by the Program for Improvement of the Research Environment for Young Researchers from the Special Coordination Funds for Promoting Science and Technology (SCF), Japan. H.N. is grateful to CREST, Japan Science and Technology Agency (JST) for funding this research. Y. K. thanks Professor Ryo Akiyama of Kyushu University for helpful discussion.

[1] G. Jones II, W. R. Jackson, C.-Y. Choi, and W. R. Bergmark, J. Phys. Chem. **89**, 24 (1985).
[2] T. L. Arbeloa, F. L. Arbeloa, M. J. Tapia, and I. L. Arbeloa, J. Phys. Chem. **97**, 4704 (1993).
[3] T. L. Arbeloa, F. L. Arbeloa, and I. L. Arbeloa, J. Lumin. **68**, 149 (1996).
[4] T. Gustavsson, T. L. Cassara, V. Gulbinas, G. Gurzadyan, J.-C. Mialocq, S. Pommeret, M. Sorgius, and P. Van Der Meulen, J. Phys. Chem. A **102**, 4229 (1998).
[5] Y. Chen, P. M. Palmer, and M. R. Topp, Int. J. Mass Spectrom. **220**, 231 (2002).
[6] V. K. Sharma, P. D. Saharo, N. Sharma, R. C. Rastogi, S. K. Ghoshal, and D. Mohan, Spectrochim. Acta, Part A **59**, 1161 (2003).
[7] S. Nad and H. Pal, J. Phys. Chem. A **105**, 1097 (2001).
[8] H. Pal, S. Nad, and M. Kumbhakar, J. Chem. Phys. **119**, 442 (2003).
[9] K. Das, B. Jain, and H. S. Patel, J. Phys. Chem. A **110**, 1698 (2006).
[10] R. S. Moog, D. D. Kim, J. J. Oberle, and S. G. Ostrowski, J. Phys. Chem. A **108**, 9294 (2004).
[11] A. Mühlpfordt, R. Schanz, N. P. Ernsting, V. Farztdinov, and S. Grimme, Phys. Chem. Chem. Phys. **1**, 3209 (1999).
[12] P. K. McCarthy and G. J. Blanchard, J. Phys. Chem. **97**, 12205 (1993).
[13] K. Ando, J. Chem. Phys. **107**, 4585 (1997).
[14] J. Neugebauer, C. R. Jacob, T. A. Wesolowski, and E. J. Baerends, J. Phys. Chem. **109**, 7805 (2005).
[15] M. Sulpizi, U. F. Röhrig, J. Hutter, and U. Rothlisberger, Int. J. Quantum Chem. **101**, 671 (2004).
[16] R. J. Cave, K. Burke, and E. W. Castner, Jr., J. Phys. Chem. A **106**, 9294 (2002).
[17] K. A. Nguyen, P. N. Day, and R. Pachter, J. Chem. Phys. **126**, 094303 (2007).
[18] R. Improta, V. Barone, and F. Santoro, Angew. Chem. **119**, 409 (2007).
[19] M. Sulpizi, P. Carloni, J. Hutter, and U. Rothlisberger, Phys. Chem. Chem. Phys. **5**, 4798 (2003).
[20] Y. Kurashige, T. Nakajima, S. Kurashige, K. Hirao, and Y. Nishikitani, J. Phys. Chem. A **111**, 5544 (2007).
[21] D. Kina, P. Arora, A. Nakayama, T. Noro, M. S. Gordon, and T. Taketsugu, Int. J. Quantum Chem. **109**, 2308 (2009).
[22] N. Kitamura, T. Fukagawa, S. Kohtani, S. Kitoh, K. Kunimoto, and R. Nakagaki, J. Photochem. Photobiol., A **188**, 378 (2007).
[23] T. Sakata, Y. Kawashima, and H. Nakano, Int. J. Quantum Chem. **109**, 1940 (2009).
[24] T. Sakata, Y. Kawashima, and H. Nakano, J. Phys. Chem. A **114**, 12263 (2010).
[25] A. Warshel and M. J. Levitt, J. Mol. Biol. **103**, 227 (1976).
[26] J. Gao and D. G. Truhlar, Annu. Rev. Phys. Chem. **53**, 467 (2002).
[27] A. Warshel, Annu. Rev. Biophys. Biomol. Struct. **32**, 425 (2003).
[28] A. Warshel, J. Phys. Chem. **83**, 1640 (1979).
[29] A. Warshel and A. Lappicirella, J. Am. Chem. Soc. **103**, 4664 (1981).
[30] Y. Kawashima, M. Dupuis, and K. Hirao, J. Chem. Phys. **117**, 248 (2002).
[31] J. T. Blair, K. Krogh-Jespersen, and R. M. Levy, J. Am. Chem. Soc. **111**, 6948 (1989).
[32] M. Belhadj, D. B. Kitchen, K. Krogh-Jespersen, and R. M. Levy, J. Phys. Chem. **95**, 1082 (1991).
[33] J. Kongsted, A. Osted, T. B. Pedersen, K. V. Mikkelsen, and O. Christiansen, J. Phys. Chem. A **108**, 8624 (2004).
[34] H. C. Georg, K. Coutinho, and S. Canuto, J. Chem. Phys. **123**, 124307 (2005).
[35] T. Malaspina, K. Coutinho, and S. Canuto, J. Braz. Chem. Soc. **19**, 305 (2008).
[36] M. L. Sanchez, M. A. Aguilar, and F. J. Olivares del Valle, J. Comput. Chem. **18**, 313 (1997).
[37] M. Haranczyk, M. Gutowski, and A. Warshel, Phys. Chem. Chem. Phys. **10**, 4442 (2008).
[38] S. C.. L. Kamerlin, M. Haranczyk, and A. Warshel, J. Phys. Chem. B **113**, 1253 (2009).
[39] P. Pulay and T. Janowski, Int. J. Quantum Chem. **109**, 2113 (2009).
[40] M. Strajbl, J. Forlián, and A. Warshel, J. Am. Chem. Soc. **122**, 5354 (2000).
[41] R. P. Muller and A. Warshel, J. Phys. Chem. **99**, 17516 (1995).
[42] J. Bentenzien, R. P. Muller, J. Forián, and A. Warshel, J. Phys. Chem. B **102**, 2293 (1998).
[43] M. Štrajbl, G. Hong, and A. Warshel, J. Phys. Chem. B **106**, 13333 (2002).
[44] M. H.. M. Olsson, G. Hong, and A. Warshel, J. Am. Chem. Soc. **125**, 5025 (2003).
[45] M. Klähn, S. Braun-Sand, E. Rosta, and A. Warshel, J. Phys. Chem. B **109**, 15645 (2005).
[46] E. Rosta, M. Klähn, and A. Warshel, J. Phys. Chem. B **110**, 2934 (2006).
[47] S. Sakane, E. M. Yezdimer, W. Liu, J. A. Barriocanal, D. J. Doren, and R. H. Wood, J. Chem. Phys. **113**, 2583 (2000).
[48] Y. Zhang, H. Liu, and W. Yang, J. Chem. Phys. **112**, 3483 (2000).
[49] R. Iftimie, D. Salahub, and J. Schofield, J. Chem. Phys. **119**, 11285 (2003).
[50] A. Crespo, M. A. Marti, D. A. Estrin, and A. E. Roitberg, J. Am. Chem. Soc. **127**, 6940 (2005).
[51] P. Bandyopadhyay, J. Chem. Phys. **122**, 091102 (2005).
[52] K. Hirao, Chem. Phys. Lett. **190**, 374 (1992).
[53] K. Hirao, Chem. Phys. Lett. **196**, 397 (1992).
[54] K. Hirao, Int. J. Quantum Chem. **S26**, 517 (1992).
[55] H. Nakano, J. Chem. Phys. **99**, 7983 (1993).
[56] H. Nakano, Chem. Phys. Lett. **207**, 372 (1993).
[57] K. Hirao, H. Nakano, and T. Hashimoto, Chem. Phys. Lett. **235**, 430 (1995).
[58] T. Tsuneda, H. Nakano, and K. Hirao, J. Chem. Phys. **103**, 6520 (1995).
[59] H. Nakano, T. Tsuneda, T. Hashimoto, and K. Hirao, J. Chem. Phys. **104**, 2312 (1996).
[60] H. Hashimoto, H. Nakano, and K. Hirao, J. Chem. Phys. **104**, 6244 (1996).
[61] Y. Kawashima, K. Nakayama, H. Nakano, and K. Hirao, Chem. Phys. Lett. **267**, 82 (1997).
[62] K. Nakayama, H. Nakano, and K. Hirao, Int. J. Quantum Chem. **66**, 157 (1998).
[63] T. Hashimoto, H. Nakano, and K. Hirao, J. Mol. Struct.: THEOCHEM **451**, 25 (1998).
[64] Y. Kawashima, T. Hashimoto, H. Nakano, and K. Hirao, Theor. Chem. Acc. **102**, 49 (1999).
[65] H. Nakano, R. Uchiyama, and K. Hirao, J. Comput. Chem. **23**, 1166 (2002).
[66] M. Miyajima, Y. Watanabe, and H. Nakano, J. Chem. Phys. **124**, 044101 (2006).
[67] V. Luzhkov and A. Warshel, J. Am. Chem. Soc. **113**, 4491 (1991).
[68] A. Warshel and Z. T. Chu, J. Phys. Chem. B **105**, 9857 (2001).
[69] A. D. Becke, J. Chem. Phys. **98**, 5648 (1993).
[70] A. D. Becke, Phys. Rev. A **38**, 3098 (1988).
[71] C. Lee, W. Yang, and R. G. Parr, Phys. Rev. B **37**, 785 (1988).
[72] T. H. Dunning, J. Chem. Phys **90**, 1007 (1989).
[73] T. Darden, D. York, and L. Pederson, J. Chem. Phys. **98**, 10089 (1993).
[74] A. D. MacKerell, Jr., N. Banavali, and N. Foloppe, Biopolymers **56**, 257 (2001).
[75] W. L. Jorgensen, J. Chandrasekhar, J. D. Madura, R. W. Impey, and M. L. Klein, J. Chem. Phys. **79**, 926 (1983).
[76] B. R. Brooks, C. L. Brooks III, A. D. MacKerell, L. Nilsson, R. J. Petrella, B. Roux, Y. Won, G. Archontis, C. Bartels, S. Boresch, A. Caflisch, L. Caves, Q. Cui, A. R. Dinner, M. Feig, S. Fischer, J. Gao, M. Hodoscek, W. Im, K. Kuczera, T. Lazaridis, J. Ma, V. Ovchinnikov, E. Paci, R. W. Pastor, C. B. Post, J. Z. Pu, M. Schaefer, B. Tidor, R. M. Venable, H. L. Woodcock, X. Wu, W. Yang, D. M. York, and M. Karplus, J. Comp. Chem. **30**, 1545 (2009).
[77] Y. Shao, L. Fusti-Molnar, Y. Jung, J. Kussmann, C. Ochsenfeld, S. T. Brown, A. T. B. Gilbert, L. V. Slipchenko, S. V. Levchenko, D. P. O'Neill, R. A. Distasio, Jr., R. C. Lochan, T. Wang, G. J. O. Beran, N. A. Besley, J. M. Herbert, C. Y. Lin, T. Van Voorhis, S. H. Chien, A. Sodt, R. P. Steele, V. A. Rassolov, P. E. Maslen, P. P. Korambath, R. D. Adamson, B. Austin, J. Baker, E. F.. C. Byrd, H. Dachsel, R. J. Doerksen, A. Dreuw, B. D.

Dunietz, A. D. Dutoi, T. R. Furlani, S. R. Gwaltney, A. Heyden, S. Hirata, C.-P. Hsu, G. Kedziora, R. Z. Khalliulin, P. Klunzinger, A. M. Lee, M. S. Lee, W. Liang, I. Lotan, N. Nair, B. Peters, E. I. Proynov, P. A. Pieniazek, Y. M. Rhee, J. Ritchie, E. Rosta, C. D. Sherrill, A. C. Simmonett, J. E. Subotnik, H. L. Woodcock III, W. Zhang, A. T. Bell, A. K. Chakraborty, D. M. Chipman, F. J. Keil, A. Warshel, W. J. Hehre, H. F. Schaefer III, J. Kong, A. I. Krylov, P. M. W. Gill, and M. Head-Gordon, Phys. Chem. Chem. Phys. **8**, 3172 (2006).

[78] J. C. Phillips, R. Braun, W. Wang, J. Gumbart, E. Tajkhorshid, E. Villa, C. Chipot, R. D. Skeel, L. Kale, and K. Schulten, J. Comput. Chem. **26**, 1781 (2005).

[79] M. W. Schmidt, K. K. Baldridge, J. A. Boatz, S. T. Elbert, M. S. Gordon, J. H. Jensen, S. Koseki, N. Matsunaga, K. A. Nguyen, S. Su, T. L. Windus, M. Dupuis, and J. A. Montgomery, J. Comput. Chem. **14**, 1347 (1993).

[80] A. M. Virshup, C. Punwong, T. V. Pogorelov, B. A. Lindquist, C. Ko, and T. J. Martinez, J. Phys. Chem. B **113**, 3280 (2009).